

Incorporation of iodate into uranyl borates and its implication for the immobilization of ^{129}I in nuclear waste repositories

By S. Wu¹, S. Wang², A. Simonetti², F. Chen¹ and T. E. Albrecht-Schmitt^{2,*}

¹ Guangzhou Institute of Geochemistry, Chinese Academy of Sciences, Guangzhou 510640, China

² Department of Civil Engineering and Geological Sciences and Department of Chemistry and Biochemistry, University of Notre Dame, Notre Dame, Indiana 46556, USA

(Received August 22, 2010; accepted in revised form April 23, 2011)

Iodate / Co-contaminates / I-129 / Immobilization

Summary. A series of uranyl borates, $\text{UO}_2\text{B}_2\text{O}_4$, $\text{Na}[(\text{UO}_2)_2\text{B}_6\text{O}_{10}(\text{OH})_3] \cdot 2\text{H}_2\text{O}$, and $\text{K}_2[(\text{UO}_2)_2\text{B}_{12}\text{O}_{19}(\text{OH})_4] \cdot 0.3\text{H}_2\text{O}$, with different topologies have been prepared and tested for the incorporation of iodate, one of the chemical forms that ^{129}I should have in nuclear waste. Laser ablation ICP-MS was used to determine the iodine content in single crystals of the three different uranyl borates. Iodine levels can be greater than 3200 ppm in crystals synthesized in the presence of iodate. The intercalation of iodic acid is one possible mechanism for iodate uptake in these solids.

1. Introduction

Borosilicate glasses are being used as a long-term storage material for containing used nuclear fuel and other nuclear wastes. These glasses are of different compositions and include R7T7, AVM, VRC, SNO8, and SM513 [1–3]. In order to evaluate the performance of repositories in the long term, it is necessary to study the corrosion behavior of nuclear waste. Alteration phases are expected to form during the corrosion of waste glass [4–7] and used nuclear fuel [8–12]. Uranyl borates may form during the cooling and storage of borosilicate glasses containing nuclear waste. They may also form as alteration products. A series of actinide borates have recently been prepared by a facile route in enabling subsequent physical property measurements [13–17].

Burns *et al.* [18] and Chen *et al.* [19] predicted the possibility that actinides and selenium could be incorporated into the alteration uranyl phases in trace quantities, which might be a mechanism for immobilizing ^{79}Se . Several experimental studies have confirmed that ^{237}Np can be incorporated into uranyl silicates, hydroxides, and phosphates [20–26]. Owing to its long half-life and bioavailability, ^{129}I is a radionuclide of special concern in repositories. Our previous studies have shown that ^{129}I can be incorporated into a uranyl silicate and three uranyl phosphate in the form of iodate [27, 28]. Recently, we reported the coupled substitution of Np^{5+} and iodate into a uranyl phosphate [29]. Since uranyl borates might form or be ini-

tially present in a repository [13–17], iodine uptake by these compounds is of interest. Therefore, the uptake of iodate during the formation of three typical uranyl borates, $\text{UO}_2\text{B}_2\text{O}_4$ (UB), $\text{Na}[(\text{UO}_2)_2\text{B}_6\text{O}_{10}(\text{OH})_3] \cdot 2\text{H}_2\text{O}$ (NaUB) and $\text{K}_2[(\text{UO}_2)_2\text{B}_{12}\text{O}_{19}(\text{OH})_4] \cdot 0.3\text{H}_2\text{O}$ (KUB) under mild hydrothermal conditions was investigated.

2. Experimental section

2.1 Syntheses

$\text{UO}_2(\text{NO}_3)_2 \cdot 6\text{H}_2\text{O}$ (98%, International Bio-Analytical Industries), H_3BO_3 (99.99%, Alfa-Aesar), NaNO_3 (99.3%, Fisher), KNO_3 (99.3%, Fisher), and HIO_3 (99.5%, Alfa-Aesar) were used as received without further purification. Distilled and Millipore filtered water with resistance of $18.2\text{ M}\Omega\text{ cm}$ was used in all reactions. PTFE-lined autoclaves were used for all reactions. **Caution!** *While the $\text{UO}_2(\text{NO}_3)_2 \cdot 6\text{H}_2\text{O}$ used in this study contained depleted U, there is really not much difference between depleted uranium and natural abundance uranium, and standard precautions for handling radioactive materials should be followed at all times. There are very old sources of uranyl nitrate that may not be depleted, and enhanced care is warranted for these samples.*

$\text{UO}_2\text{B}_2\text{O}_4$ (UB), $\text{Na}[(\text{UO}_2)_2\text{B}_6\text{O}_{10}(\text{OH})_3] \cdot 2\text{H}_2\text{O}$ (NaUB), and $\text{K}_2[(\text{UO}_2)_2\text{B}_{12}\text{O}_{19}(\text{OH})_4] \cdot 0.3\text{H}_2\text{O}$ (KUB) were synthesized using the methods of Wang *et al.* [15–17] with molar ratios of B : U = 8 : 1 in UB, Na : B : U = 5 : 15 : 1 in NaUB and K : B : U = 5 : 15 : 1 in KUB. All autoclaves were sealed and heated to $190\text{ }^\circ\text{C}$ in a box furnace for 2 d. UB, NaUB and KUB were the same compounds as UBO-1, NaUB4, and KUBO-1, respectively, in Wang *et al.*'s paper [15–17].

2.2 Incorporation of iodate into uranyl borate

In order to compare iodate uptake by crystals grown in the presence of iodate vs. those grown in the absence of iodate but added back into iodate solutions, two series experiments were designed as follows: (1) UB, NaUB, and KUB were synthesized in the presence of HIO_3 with the U:I molar ratios of 20 : 1 and 10 : 1, respectively, and the synthesized compounds were labeled as UB1, UB2, NaUB1, NaUB2,

* Author for correspondence (E-mail: talbrec1@nd.edu).

KUB1, and KUB2, respectively; (2) 0.0050 g, 0.0350 g, and 0.0053 g of synthesized iodine-free UB, NaUB, and KUB were reacted, respectively, with suitable amounts of boric acid and iodic acid solutions under mild hydrothermal condition. The molar ratios of uranium to borate were as same as that in (1) and the molar ratios of uranium to iodate in all reactions were kept at 20:1 and 10:1, respectively. Other procedures were same as (1). The samples were labeled as UB3, UB4, NaUB3, NaUB4, KUB3, and KUB4, respectively. And the volumes of iodic acid solution are 100, 200, 25, 50, 5 and 10 μL for UB3, UB4, NaUB3, NaUB4, KUB3, and KUB4, respectively. The iodate-bearing samples were washed and dried using the same method as that used by Wang *et al.* [15–17]. ^{127}I was used as an analogue for ^{129}I in this study.

2.3 Powder X-ray diffraction

Powder X-ray diffraction patterns of all products were collected on a Scintag $\theta-\theta$ diffractometer equipped with a diffracted-beamed monochromatic set for $\text{Cu } K_{\alpha}$ ($\lambda = 1.54056 \text{ \AA}$) radiation at room temperature in the angular range from 5° to 80° (2θ) with a scanning step width of 0.05° and a fixed counting time of 1 s/step.

2.4 Crystallographic studies

Single crystals of all samples were selected and mounted on glass fibers with epoxy and aligned on a Bruker APEXII Quazar CCD X-ray diffractometer with a digital camera to determine unit cell parameters. The unit cells of iodine-incorporated samples were checked prior to Laser-Ablation Inductively Coupled Plasma Mass Spectrometer (LA-ICP-MS) analysis.

2.5 LA-ICP-MS analysis

The iodine and uranium contents of the experiment products were analyzed using a ThermoFinnigan high resolution magnetic sector Element2 ICP-MS instrument coupled to a UP213 Nd:YAG laser ablation system (New Wave Research). Selected crystals were fixed on 1-inch glass slides with double-sided tape. Individual analyses consisted of a 60 s measurement of background ion signals followed by a 60 s interval of measurement of ion signals subsequent the start of lasering. Each analysis represents a total of 93 scans ($93 \text{ runs} \times 1 \text{ pass}$) with a sample (dwell) time of 0.01 s with 20 samples per ion signal peak. Analyses were conducted in medium mass resolution mode (resolution = mass/peak width ~ 4000) in order to eliminate possible spectral interferences. The ablated particles were transported from the ablation cell to the ICP-MS instrument using He carrier gas at a flow rate of 0.7 L/min. Crystals were ablated using a range of spot sizes between 40 to 55 μm , repetition rate of 2 Hz and 70% power output corresponding to an energy density of 12–15 J/cm^2 . This typically results in a depth of penetration of between 5 to 15 μm [30, 31]. Because of the high uranium content in the crystals, ^{235}U was monitored in order to determine the elemental ratios. The total uranium content was calculated according to the abundance of ^{235}U in the depleted uranium used in this investigation (0.35%). Based on the known U content in UB, NaUB, and KUB,

the iodine concentrations were estimated using the measured count rates (cps) of the mass spectrometer and calculated I/U ratio.

3. Results and discussion

3.1 Structures descriptions

The structures of UB, NaUB, and KUB are shown in Fig. 1. UB is light yellow and NaUB is yellow-green, and their structures have been reported recently by Wang *et al.* [15, 16]. UB is composed of $(\text{BO}_2)_1\infty 1\text{D}$ zigzag-like chains and UO_8 hexagonal bipyramids *via* edge-sharing

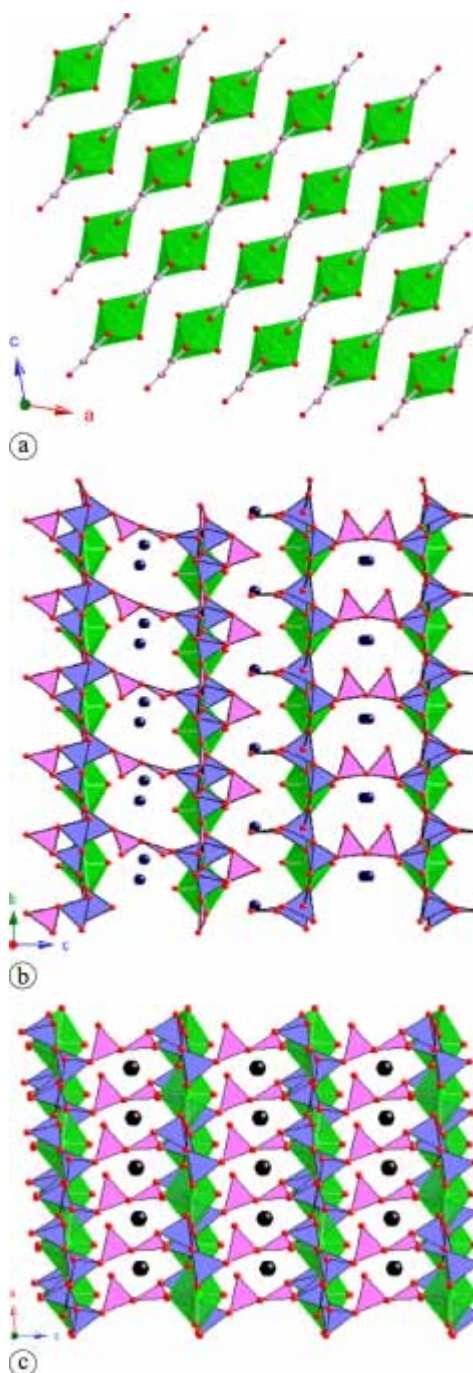
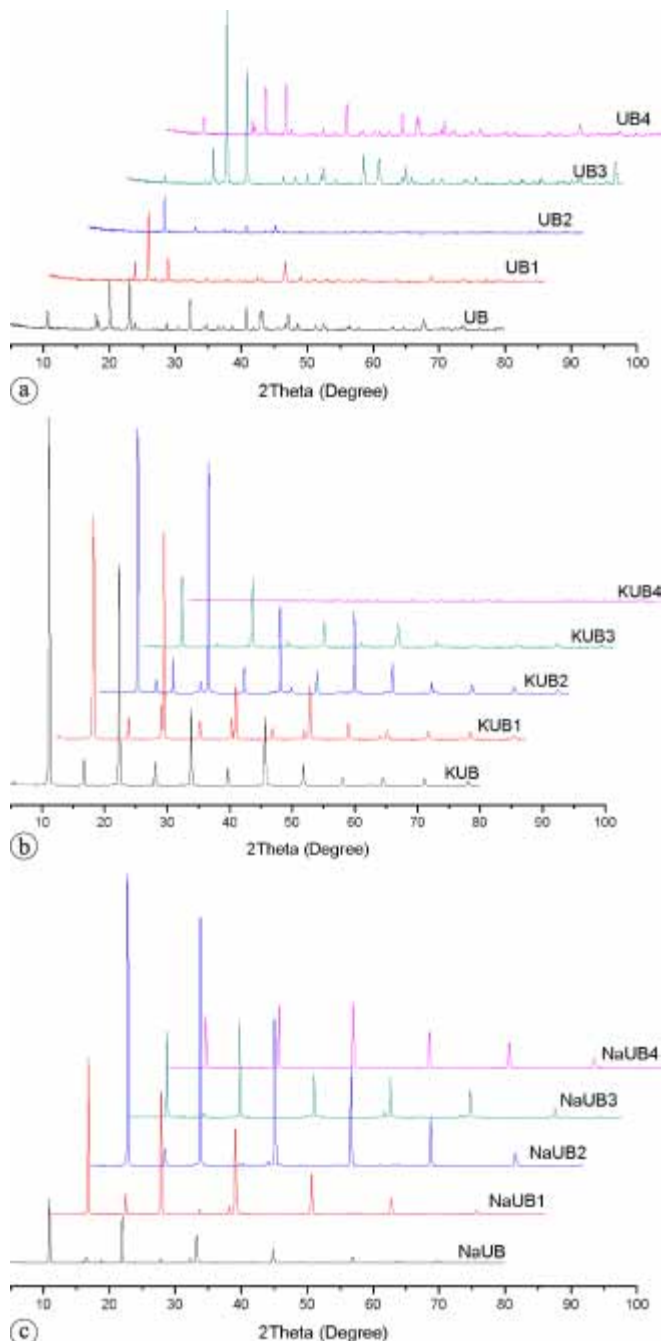


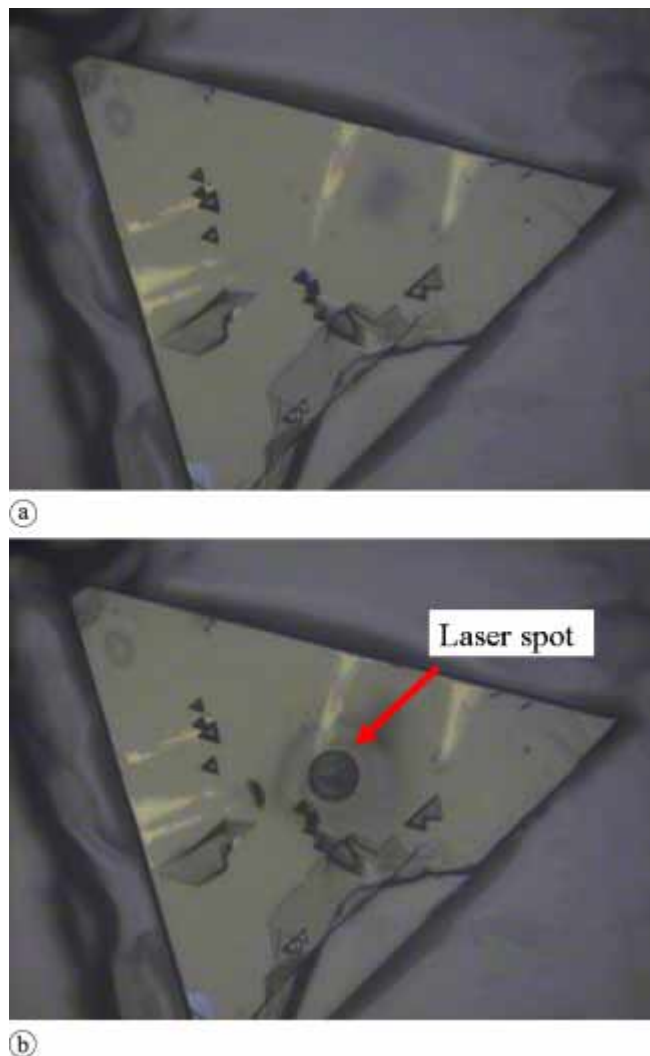
Fig. 1. General views of the structure of UB (a), KUB (b) and NaUB (c). UO_8 hexagonal bipyramids are shown in green, BO_3 units in pink, BO_4 units in purple, K and Na cations in black and O anions in red.

Table 1. Crystallographic information of UB, NaUB, KUB and uranyl iodate.

Sample	Color	$a(\text{\AA})$	$b(\text{\AA})$	$c(\text{\AA})$	$\beta(^{\circ})$	$V(\text{\AA}^3)$	Space group	Reference
UB	Yellow	10.46	4.19	15.63	109.77	231.81	$C2$	[15]
NaUB	Yellow	6.39	11.14	15.99	92.77	1136.7	Cc	[16]
KUB	Yellow-green	6.43	6.43	47.43	120	1699.8	$P3_112$	[17]
Uranyl iodate	Yellow	8.45	7.71	12.27	90	799.3	$Pbcn$	[32]

**Fig. 2.** Powder X-ray patterns of UB, KUB and NaUB and the iodate incorporated samples.

to form 2D layer [15]. It is remarkable that there are no cations or water molecules between the sheets (Fig. 1a), thus these sheets are held together only by van der Waals forces. KUB is based on double, negatively charged layers united in regular 3D structure by potassium cations distributed in the interlayer space [17]. It is interesting that KUB has

**Fig. 3.** Photomicrograph of KUB crystal before (a) and after (b) laser ablation.

a yellow-green color and the crystals adopt a triangular habit. The color does not change when iodine is incorporated into the structure. The basic structure of NaUB is composed of uranyl bipyramids, BO_3 and BO_4 polyhedra, which is similar to KUB. However, each uranyl cation in NaUB was surrounded by B_9O_{24} to form ${}_{\infty}^3[(\text{UO}_2)(\text{B}_6\text{O}_{10})(\text{OH})]^-$ framework which is not found in UB and KUB. Na^+ cations and water were found within the pores of framework [16]. The detailed structures of UB, NaUB, and KUB have been reported by Wang *et al.* [15–17].

3.2 Chemical phases

The XRD patterns of all products were shown in Fig. 2. The patterns of samples synthesized in iodate-free systems are

Table 2. Concentration of iodine in uranyl borate.

Sample	I/U (molar)	Iodine (ppm)
UB1	0.00751	2011.72
UB3	0.00071	253.19
UB4	0.00899	3211.38
KUB1	2.22×10^{-6}	0.33
KUB2	2.02×10^{-5}	4.60
KUB3	5.78×10^{-6}	1.31
NaUB1	1.38×10^{-6}	0.31
NaUB2	0.00050	111.92
NaUB3	5.66×10^{-6}	1.26
NaUB4	4.48×10^{-6}	0.99

identical to those reported by Wang *et al.* [15–17] for UB, NaUB, and KUB, respectively, indicating that pure phases of these compounds were obtained. On the other hand, when iodate was present, some undesired phases were observed in UB1, UB2, and KUB4 and were analyzed using electron microscope and single crystal XRD. Sample UB1 consists of $UO_2B_2O_4$ and uranyl iodate, $UO_2(IO_3)_2(H_2O)$, while samples UB2 and KUB4 are pure uranyl iodate, which indicates that iodate is a strong ligand that may substitute for borate in uranyl phases if the structure is feasible. The presence of $UO_2(IO_3)_2(H_2O)$ was identified using electron microscope

and single crystal XRD. The unit cell parameters of each crystal were listed in Table 1.

3.3 LA-ICP-MS

LA-ICP-MS is well-suited for *in situ* chemical analysis of trace element in small crystals, and hence was used to detect the incorporated iodine within the synthesized uranyl borate crystals. Our previous studies have shown that this method can supply information on the chemical makeup of crystals at high spatial resolution ($\sim 50 \mu\text{m}$ wide at surface and $\sim 15 \mu\text{m}$ depth; Fig. 3). Obviously, such information cannot be obtained by bulk sample digestion and subsequent solution mode analysis. As shown in the time-resolved laser ablation spectrum (Fig. 4), background ion signals are very low and smooth prior the start of laser. Subsequent laser, ^{127}I ion signals were detected, in particular for crystals UB1 and UB4 (Fig. 4) indicating that iodine was incorporated into these crystals. The average molar I/U ratios and the calculated iodine concentrations are listed in Table 2.

Samples UB2 and KUB4 are pure uranyl iodate phases and thus were not analyzed by LA-ICP-MS. For the analysis of the uranyl borates, single crystals were hand-picked carefully using a binocular microscope and verified with single

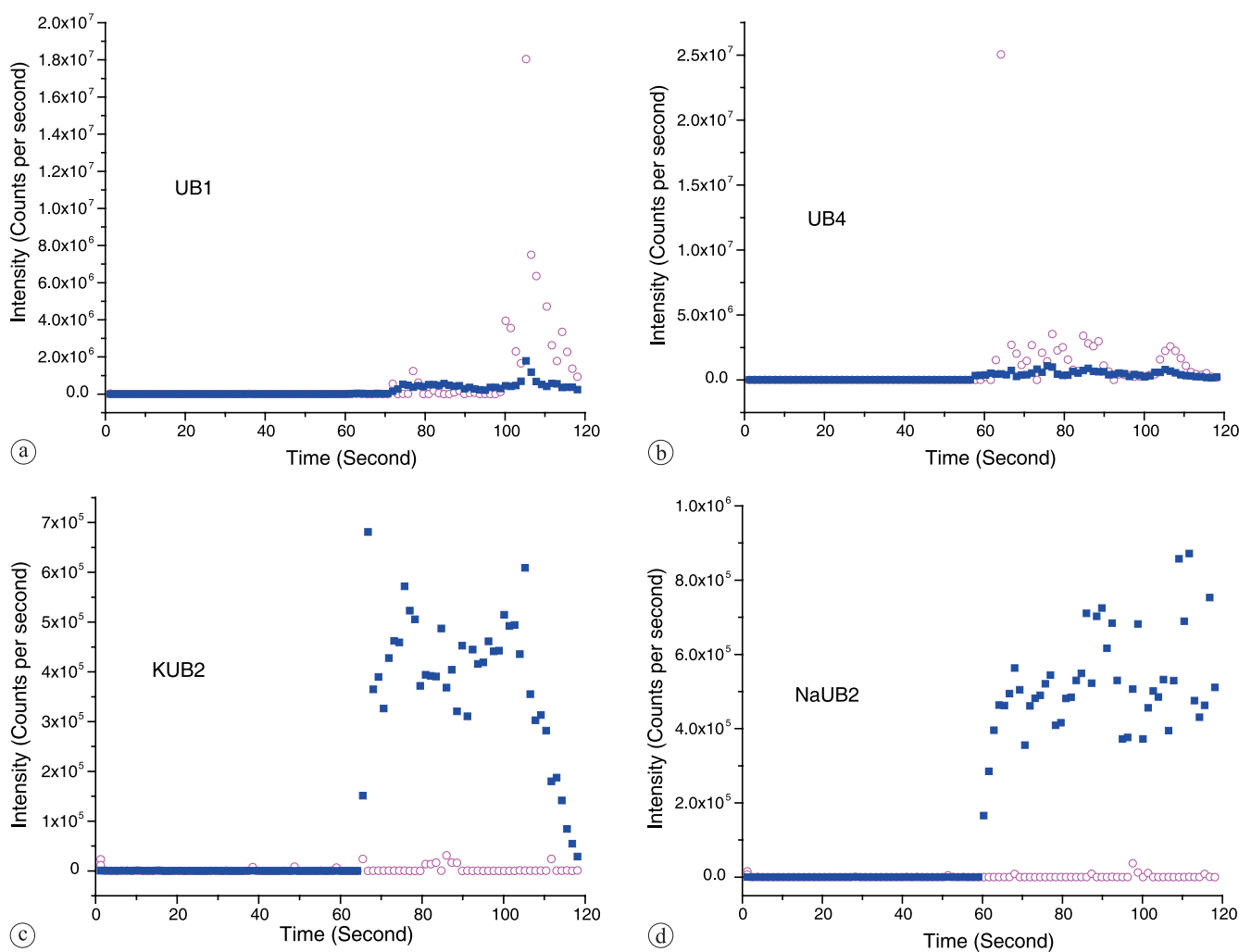
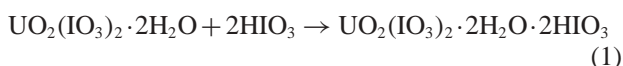


Fig. 4. Typical LA-ICP-MS spectrum for UB1, UB4, NaUB2 and KUB2. ^{127}I was shown in open circle and ^{235}U in square.

XRD. Generally, the incorporated iodine in UB ranges from 253.19 ppm to 3211.38 ppm, contrasting with 0.33 ppm to 4.60 ppm in KUB.

As is discussed in our previous study, IO_3^- trigonal pyramid could substitute for PO_4^{3-} tetrahedron if there is a terminal oxygen in PO_4^{3-} [28, 29]. If this rule can be used in uranyl borates, the iodine concentration in KUB should be much higher than that in UB because KUB has terminal oxygen in BO_3 polyhedra. Based on the LA-ICP-MS data, it is unlikely that BO_3 polyhedra are substituted for by IO_3^- anions. The trace amount of iodine in KUB samples may be contributed by iodine inclusion, or intercalated between the layers. Generally, anions with similar valences and geometries can easily substitute for one another, such as $(\text{IO}_4^-)(\text{OH}^-)_2 \leftrightarrow (\text{SiO}_4\text{OH})_3^-$ and $\text{IO}_3^- \leftrightarrow \text{HPO}_4^{2-}$ [27, 28]. However, the length of I–O bond ranges between 1.77 Å and 1.86 Å and is much longer than the B–O bond (1.36–1.49 Å). This may therefore account for the very limited substitution between IO_3^- and BO_3 or BO_4 polyhedra in uranyl borates.

Ling and Albrecht-Schmitt demonstrated the intercalation of iodic acid into the layered uranyl iodate to yield $\text{UO}_2(\text{IO}_3)_2 \cdot 2\text{H}_2\text{O} \cdot 2\text{HIO}_3$ in crystalline form, and the reaction was described by the following equation [33].



As described above, there is no direct linkage between adjacent sheets, which are held together only by van der Waals forces. In addition, the interlayer space within UB is about 2 Å, which is large enough for the emplacement of HIO_3 molecules. Thus, the intercalation mechanism of iodate into UB is expected, which accounts for the substantial iodine detected in samples UB1, UB3 and UB4. The intercalation of HIO_3 into UB layers can be described as follows.



According to the experiments conducted by Ling and Albrecht-Schmitt, when large excess iodic acid is present, $\text{UO}_2(\text{IO}_3)_2 \cdot 2\text{H}_2\text{O}$ will transform into a new structure, $\text{UO}_2(\text{IO}_3)_2 \cdot 2\text{H}_2\text{O} \cdot 2\text{HIO}_3$ [33]. In this study, pure uranyl borate (UB2) was synthesized when U:I ratio at 10:1, but phase transformation did not occur in UB4 when UB reacted with iodate-bearing solution under similar conditions.

The iodine ion signals within KUB and NaUB are concentrated within a few seconds of the ablation interval; a feature that is characteristic of when ablating crystals containing inclusions. As the laser hits an iodine-containing inclusion, the mass spec records some iodine and the remaining part of the interval is blank. This is precisely what is shown in the time-resolved spectra.

In the reported iodate substitution, both the SiO_4 and PO_4 polyhedra are isolated with other SiO_4 or PO_4 polyhedra [27–29]. In contrast, the BO_3 or BO_4 polyhedra in KUB and NaUB structure are connected to other BO_3 or BO_4 polyhedra to form framework. And in UB the BO_3 polyhedra are connected to other BO_3 to form $(\text{BO}_2)_1\infty 1\text{D}$ zigzag-like chains. Thus, the substitutions of $\text{IO}_3 \leftrightarrow \text{BO}_3$ or $\text{IO}_3 \leftrightarrow \text{BO}_4$

will disrupt the structural connectivity and are unlikely to occur.

3.4 Implication for the immobilization of ^{129}I in nuclear waste repositories

One of the structural characteristics of $\text{UO}_2(\text{IO}_3)_2 \cdot 2\text{H}_2\text{O}$ and $\text{UO}_2\text{B}_2\text{O}_4$ is that the space between the sheets is empty, which is easily filled by other neutral molecules. In this case, the intercalated molecule is HIO_3 . As shown in Fig. 5, the structure of rutherfordine, UO_2CO_3 [34], as well as UO_2SeO_3 [35], and UO_2TeO_3 [36] also have unoccupied spaces between the sheets. Considering the similarity of the

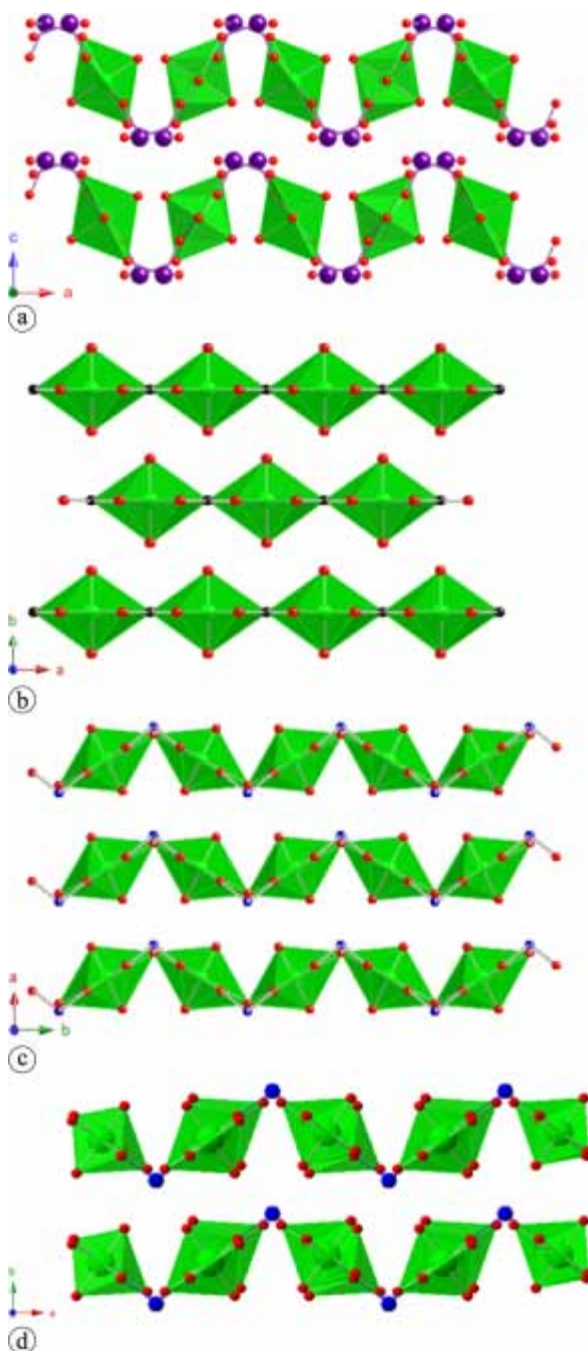


Fig. 5. Views of the structure of $\text{UO}_2(\text{IO}_3)_2(\text{H}_2\text{O})$ (a), UO_2CO_3 (b), UO_2SeO_3 (c) and UO_2TeO_3 (d). UO_8 hexagonal bipyramids are shown in green, Se and Te in blue and O in red.

structure, the intercalation of iodic acid into the layers of UO_2CO_3 , UO_2SeO_3 , UO_2TeO_3 and other similar structures is also expected, but experimental investigation is required. Therefore, intercalation may be a plausible mechanism for immobilizing ^{129}I in nuclear waste repositories.

4. Conclusions

As one of the forms for disposing of high level waste, borosilicate glass is very important for immobilizing the radionuclides in repositories. Uranyl borate may be initially present or form during the long-term storage and subsequent alteration. According to the differences of bond distances between IO_3 and BO_3 and different geometry, it is unlikely that IO_3 will substitute for BO_3 polyhedra in uranyl borates. Furthermore, IO_3 units will not substitute for BO_4 based on the LA-ICP-MS results. The trace iodine found in KUB and NaUB should be contributed by iodine inclusion while iodine may intercalate in significant level into layered UB in the form of iodic acid. It is expected that iodic acid can also incorporate into the interlayers of some layered structures such as UO_2CO_3 , UO_2SeO_3 , and UO_2TeO_3 .

Acknowledgment. We are grateful for support provided by the Office of Civilian Radioactive Waste Management (USA), Office of Science and Technology and International, through a subcontract with Argonne National Laboratory, and the National Natural Science Foundation of China (Grant No. 40972213).

References

- Frugier, P., Martin, C., Ribet, I., Advocat, T., Gin, S.: The effect of composition on the leaching of three nuclear waste glasses: R7T7, AVM and VRZ. *J. Nucl. Mater.* **346**, 194 (2005).
- Abdelouas, A., Crovisier, J.-L., Lutze, W., Grambow, B., Dran, J.-C., Müller, R.: Surface layers on a borosilicate nuclear waste glass corroded in MgCl_2 solution. *J. Nucl. Mater.* **240**, 100 (1997).
- Lodding, A., Isegheem, P. V.: In-depth distributions of elements in leached layers on two HLW waste glasses after burial in clay; step-scan by SIMS. *J. Nucl. Mater.* **298**, 197 (2001).
- Abdelouas, A., Crovisier, J.-L., Lutze, W., Müller, R., Bernotat, W.: Structure and chemical properties of surface layers developed on R7T7 simulated nuclear waste glass altered in brine at 190 °C. *Eur. J. Mineral.* **7**, 1101 (1995).
- Abdelouas, A., Crovisier, J.-L., Lutze, W., Fritz, B., Mosser, A., Müller, R.: Formation of hydrotalcite-like compounds during R7T7 nuclear waste glass and basaltic glass alteration. *Clays Clay Miner.* **42**, 526 (1994).
- Abrajano, T. A., Bates, J. K., Woodland, A. B., Bradley, J. P., Bourcier, W. L.: Secondary phase formation during nuclear waste-glass dissolution. *Clays Clay Miner.* **38**, 537 (1990).
- Vernaz, E., Gin, S., Jégou, C., Ribet, I.: Present understanding of R7T7 glass alteration kinetics and their impact on long-term behavior modeling. *J. Nucl. Mater.* **298**, 27 (2001).
- Wronkiewicz, D. J., Bates, J. K., Wolf, S. F., Buck, E. C.: Ten-year results from unsaturated drip tests with UO_2 at 90 °C: Implications for the corrosion of spent nuclear fuel. *J. Nucl. Mater.* **238**, 78 (1996).
- Buck, E. C., Wronkiewicz, D. J., Finn, P. A., Bates, J. K.: A new uranyl oxide hydrate phase derived from spent fuel alteration. *J. Nucl. Mater.* **249**, 70 (1997).
- Forsyth, R. S., Werme, L. O.: Spent fuel corrosion and dissolution. *J. Nucl. Mater.* **190**, 3(1992).
- Wronkiewicz, D. J., Bates, J. K., Gerding, T. J., Veleckis, E., Tani, B. S.: Uranium release and secondary phase formation during unsaturated testing of UO_2 at 90 °C. *J. Nucl. Mater.* **190**, 107(1992).
- Finch, R. J., Ewing, R. C.: The corrosion of uraninite under oxidizing conditions. *J. Nucl. Mater.* **190**, 133 (1992).
- Wang, S., Alekseev, E. V., Diwu, J., Casey, W. H., Phillips, B. L., Depmeier, W., Albrecht-Schmitt, T. E.: NDTB-1: A supertetrahedral cationic framework that removes TcO_4^- from solution. *Angew. Chem. Int. Ed.* **49**, 1057 (2010).
- Wang, S., Alekseev, E. V., Ling, J., Skanthakumar, S., Soderholm, L., Depmeier, W., Albrecht-Schmitt, T. E.: Neptunium diverges sharply from uranium and plutonium in crystalline borate matrixes: Insights into the complex behavior of the early actinides relevant to nuclear waste storage. *Angew. Chem. Int. Ed.* **49**, 1263 (2010).
- Wang, S., Alekseev, E. V., Stritzinger, J. T., Depmeier, W., Albrecht-Schmitt, T. E.: How are centrosymmetric and noncentrosymmetric structures achieved in uranyl borates? *Inorg. Chem.* **49**, 2948 (2010).
- Wang, S., Alekseev, E. V., Ling, J., Liu, G., Depmeier, W., Albrecht-Schmitt, T. E.: Polarity and chirality in uranyl borates: Insights into understanding the vitrification of nuclear waste and the development of nonlinear optical materials. *Chem. Mater.* **22**, 2155 (2010).
- Wang, S., Alekseev, E. V., Stritzinger, J. T., Depmeier, W., Albrecht-Schmitt, T. E.: Crystal chemistry of the potassium and rubidium uranyl borate families derived from boric acid fluxes. *Inorg. Chem.* **49**, 6690 (2010).
- Burns, P. C., Ewing, R. C., Miller, M. L.: Incorporation mechanisms of actinide elements into the structures of U^{6+} phases formed during the oxidation of spent nuclear fuel. *J. Nucl. Mater.* **245**, 1 (1997).
- Chen, F., Burns, P. C., Ewing, R. C.: Se-79: geochemical and crystallo-chemical retardation mechanisms. *J. Nucl. Mater.* **275**, 81 (1999).
- Burns, P. C., Deely, K. M., Skanthakumar, S.: Neptunium incorporation into uranyl compounds that form as alteration products of spent nuclear fuel: Implications for geologic repository performance. *Radiochim. Acta* **92**, 151 (2004).
- Finch, R. J., Fortner, J. A., Buck, E. C., Wolf, S. F.: Neptunium incorporation into uranium(VI) compounds formed during aqueous corrosion of neptunium-bearing uranium oxides. *Mater. Res. Soc. Symp. Proc.* **713**, 647 (2002).
- Buck, E. C., McNamara, B. K., Douglas, M., Hanson, B. D.: Possible incorporation of neptunium in uranyl (VI) alteration phases. PNNL-14277, Pacific Northwest National Laboratory, Richland (2003).
- Douglas, M., Clark, S. B., Friese, J. I., Arey, B. W., Buck, E. C., Hanson, B. D.: Neptunium(V) partitioning to uranium(VI) oxide and peroxide solids. *Environ. Sci. Technol.* **39**, 4117 (2005).
- Klingensmith, A. L., Burns, P. C.: Neptunium substitution in synthetic uranophane and soddyite. *Am. Mineral.* **92**, 1946 (2007).
- Klingensmith, A. L., Deely, K. M., Kinman, W. S., Kelly, V., Burns, P. C.: Neptunium incorporation in sodium-substituted metaschoepite. *Am. Mineral.* **92**, 662 (2007).
- Klingensmith, A. L.: Np^{3+} incorporation into select uranyl phases and thermal analysis of select uranyl phases. University of Notre Dame, Notre Dame (2008).
- Wu, S., Chen, F., Kang, M., Yang, Y., Dou, S.: Incorporation of iodine into uranophane formed during the corrosion of spent nuclear fuel. *Radiochim. Acta* **97**, 459 (2009).
- Ling, J., Wu, S., Chen, F., Simonetti, A., Shafer, J. T., Albrecht-Schmitt, T. E.: Does iodate incorporate into layered uranyl phosphates under hydrothermal conditions? *Inorg. Chem.* **48**, 10995 (2009).
- Wu, S., Chen, F., Simonetti, A., Albrecht-Schmitt, T. E.: Incorporation of neptunium(V) and iodate into a uranyl phosphate: Implications for mitigating the release of ^{237}Np and ^{129}I in repositories. *Environ. Sci. Technol.* **44**, 3192 (2010).
- Simonetti, A., Heaman, L. M., Chacko, T., Banerjee, N. R.: *In-situ* petrographic thin section U-Pb dating of zircon, monazite, and titanite using laser ablation-MC-ICP-MS. *Int. J. Mass Spectrom.* **253**, 87 (2006).
- Simonetti, A., Heaman, L. M., Chacko, T.: Use of discrete-dynode secondary electron multipliers with Faradays – A 'reduced vol-

- ume' approach for *in-situ* U-Pb dating of accessory minerals within petrographic thin section by LA-MC-ICP-MS. In: *2008 V.M. Goldschmidt Laser Ablation Short Course 40*. (Sylvester, P., ed.) Vancouver (2008), p. 241.
32. Bean, A. C., Peper, S. M., Albrecht-Schmitt, T. E.: Structural relationships, interconversion, and optical properties of the uranyl iodates, $\text{UO}_2(\text{IO}_3)_2$ and $\text{UO}_2(\text{IO}_3)_2(\text{H}_2\text{O})$: A comparison of reactions under mild and supercritical conditions. *Chem. Mater.* **13**, 1266 (2001).
33. Ling, J., Albrecht-Schmitt, T. E.: Intercalation of iodic acid into the layered uranyl iodate, $\text{UO}_2(\text{IO}_3)_2(\text{H}_2\text{O})$. *Inorg. Chem.* **46**, 346 (2007).
34. Finch, R. J., Cooper, M. A., Hawthorne, F. C.: Refinement of the crystal structure of Rutherfordine. *Can. Mineral.* **37**, 929 (1999).
35. Loopstra, B. O., Brandenburg, N. P.: Uranyl selenite and uranyl tellurite. *Acta Cryst. B* **34**, 1335 (1978).
36. Meunier, G., Galy, J.: Structure cristalline de la schmitterite synthétique UTeO_5 . *Acta Cryst. B* **29**, 1251 (1973).